SUPPORTING INFORMATION

The Owl Sensor: a 'Fragile' DNA Nanostructure for Analysis of Single Nucleotide Variations

Rebekah J. Karadeema,[†⊥]* Maria Stancescu,† Tyler P. Steidl,[†] Sophia C. Bertot, [†] and Dmitry M. Kolpashchikov[†‡*]

[†]Chemistry Department, University of Central Florida, Orlando, FL 32816, USA.

[⊥]Current address: Department of Chemistry, The Scripps Research Institute, 10550 North Torrey Pines Road, La Jolla, California 92037, United States

⊥Burnett School of Biomedical Sciences, University of Central Florida, Orlando, 32816, Florida, USA

E-mail: rebekah@scripps.edu; dmitry.kolpashchikov@ucf.edu

Table of Contents

1. Materials and Methods

Reagents. All buffers and stock solutions were made with DNAse/protease-free water purchased from Fisher Scientific Inc. (Pittsburg, PA). All other reagents needed for buffers were purchased from Sigma-Aldrich (St. Louis, MO). The **UMB1** was custom-made by TriLink Biotechnologies, Inc. (San Diego, CA). All other oligonucleotides (sequences listed in SI Table 7) were obtained from Integrated DNA Technologies, Inc. (Coraville, IA). The concentrations of nucleic acid strands were determined using the Beer-Lambert law, a 1 cm quartz cuvette (volume of 100 μL), and extinction coefficients determined by using OligoAnalyzer 3.1 software (Integrated DNA Technologies, Inc.). Three independent and different amounts of the same oligonucleotide were mixed with water to total volume of 100 μL and tested for their absorbance values at 260 nm using a Perkin-Elmer Lambda 35 UV/Vis spectrometer (San Jose, CA). The average of the concentrations calculated was used with relative standard deviations of each sample less than 10%. Working stock solutions of convenience concentrations were prepared for all sequences and stored frozen at -20°C until use.

Melt Curve Fluorescent Assays. Prior to mixing, stock solutions of oligonucleotides were allowed to thaw to room temperature, vortexed for 5 s, and centrifuged on a tabletop minicentrifuge for 10 s. A master mix solution containing R_X/P_Y was created such that adding 11.5 μL of the master mix to the samples (to a total volume of 25 μL) would result in $\mathbf{R_X}$ and $\mathbf{P_Y}$ concentrations of 150 nM and 200 nM, respectively. For miDNA/RNA analytes, $\mathbf{R_{x\_mi}}$ and $\mathbf{P_{y\_mi}}$ concentrations were 1 μM and 200 nM, respectively. The master mix was used to make samples with the following names: Control, Mismatched, Matched, and Insertion and Deletion, if tested. The master mix solution (11.5 μL) was added to a 96-well plate (30 μL wells). Next, 1 μL of water, matched, mismatched, **Inh_del**, or **Inh_ins** was added to the plate to make the Control, Mismatched, Matched, Deletion, or Insertion samples, respectively so that the final concentration of the analyte was 100 nM. Another well was filled with 12.5 μL of water to serve as a control named 'UMB'.

The buffer used contained 50 mM Tris-HCl, pH 7.4, 50 mM $MgCl_2$, and 0.1% Tween-20 with the **UMB** and ROX unless otherwise specified. A buffer-fluorophore solution containing 2X Buffer, 100 nM **UMB** and ROX was made. By adding 12.5 μL of the buffer-fluorophore solution to each sample well, final concentrations of the fluorophores were 50 nM. ROX was used as a passive dye reference since its fluorescence shows little fluctuation with temperature. Using ROX also allows for correction of well-to-well and plate-to-plate variations in fluorescence detection. Fluorescence was reported as F_{FAM}/F_{ROX}, where F_{FAM} is the fluorescence given off by the fluorophore attached to **UMB1** and F_{ROX} is the fluorescence of the ROX reference dye.

After samples were made, an optical adhesive cover was placed firmly on top of the plate and a tool was used to seal the wells. The plate was flicked to eliminate any formed bubbles, vortexed, and then spun at 660 rcf for 20 s. The solutions were placed in the QuantStudio™ 6 Flex System and cooled (2°C/s) from room temperature to 5°C where they were annealed for 60 min. The fluorescence of the samples was then read continuously as the samples were heated (0.1°C/s) from 5°C to 95°C. The QuantStudio™ 6 Flex System software allowed for the selection of FAM™ dye to be read as the 'Target' and if ROX was utilized, it was selected as a 'Passive Reference'. The system was routinely calibrated for well factors, background, and dye fluorescence. It is important to note that samples taken after different calibrations of the system showed altered background fluorescence of UMB and the Control samples (with no analyte present); thus depending on the date the experiment was conducted, some variation in fluorescent values between experiments may be observed. The QuantStudio™ Real-Time

PCR Software (version 1.1) allows for real-time data analysis for initial processing, but all relevant data was exported to Excel for further analysis. The readings from at least two wells were averaged and replotted to produce the presented figures. The derivative of fluorescence over time was calculated by the QuantStudio™ Real-Time PCR Software. The maximum of the derivative plots gives the inflection point of the curve, also called the melting temperature (T_m).

Kinetic Studies. The concentration of Owl Sensor strands were the same as previously mentioned for fluorescent assays. To see how the Owl Sensor behaves over 24 hrs at one temperature, an altered protocol was required. Because more change in fluorescence is observed right after mixing, data was collected every 20 or 30 s for the first 1-2 hours. After that, longer periods of time were given between fluorescent readings (20 to 30 min) until 24 hrs had passed. This was achieved through 2 PCR stages. The first stage cooled the samples from 25°C to the desired temperature at 1.6°C/s. The temperature was then kept constant as the system repeatedly recorded fluorescent readings at short intervals (20 to 30 s between readings). The second PCR stage remained at the same temperature as the first and fluorescent readings were repeatedly recorded at slower intervals (20 to 30 min). Data was exported to Excel and analyzed.

Limit of Detection. The limit of detection (LOD) was determined by conducting fluorescence experiments using a 100 μL quartz in a Perkin-Elmet (San Jose, CA) LS-5S Luminescence Spectrophotometer with a Hamamatsu xenon lamp (λ_{ex} = 485 nm, λ_{em} = 517 nm). A buffer containing 50 mM Tris-HCl, pH 7.4, 50 mM $MgCl_2$, and 0.1% Tween-20 was used. Samples were incubated in 5°C water bath for 1 hr. Samples were then taken out of the bath and analyzed in the Perkin-Elmet LS-5S Luminescence Spectrophotometer at room temperature. Fluorescent values at 517 nm were recorded. Three independent trials for each sample were averaged and plotted in Excel with error bars indicating one standard deviation. The LOD was determined by calculating the signal of the control (0 nM of analyte) + 3*(standard deviation of the control).

2. ***Table S1.*** Oligonucleotide sequences used in the study.

Name	Sequence	Purification
inhT (DNA)	5'—GCG GCA TGG GTA TGG GCC ACT GAC ATA ACA CAA GGA C	SD
inhC (DNA)	5'—GCG GCA TGG GTA TGG GCC ACT GAC ACA ACA CAA GGA C	SD
inhT (RNA)	5'—GCG GCA UGG GUA UGG GCC ACU GAC AUA ACA CAA GGA C	SD
inhC (RNA)	5'—GCG GCA UGG GUA UGG GCC ACU GAC ACA ACA CAA GGA C	SD
inh_ins	5'—GCG GCA TGG GTA TGG GCC ACT GAC ACCA ACA CAA GGA C	SD
inh_del	5'—GCG GCA TGG GTA TGG GCC ACT GAC A_A ACA CAA GGA C	SD
inhT_Q	5'—GCG GCA TGG GTA TGG GCC ACT GAC ATA ACA CAA GGA C/BHQ1/	HPLC
inhC_Q	5'—GCG GCA TGG GTA TGG GCC ACT GAC ACA ACA CAA GGAC/BHQ1/	HPLC
Linear Probe	/FAM/5'—TCT TGT GTT GTG TCA GTG A	HPLC
MB Probe	/FAM/5'—CGCTC TTG TGT TGT GTC AGT GAGCG/BHQ1/	HPLC
UMB1	/FAM/5'—CGCG TTAA CATA CAAT AGAT CGCG/BHQ1/	SD
R_{12}	5'—CTATTG AGTGG CCCATA CGCGATC	SD
P_{12}	5'—AACGCG TTGTGT TGTGTC TATGTT	SD
R_{11}	5'—TATTG AGTGG CCCATA GCGATC	SD
P_{11}	5'—TAACGC TGTGTT GTGTC TATGT	SD
R_{10}	5'—TATTG AGTGG CCCAT CGATC	SD
P_{10}	5'—TAACG GTGTT GTGTC TATGT	SD
R_{9}	5'—TATTG AGTGG CCCA GATC	SD
P_{9}	5'—TAAC TGTT GTGTC TATGT	SD
P_{9_A}	5'—TAAC TGTT GTATC TATGT	SD
R_{8}	5'—ATTG AGTG GCCC ATCT	SD
P_{8}	5'—TTAA GTTG TGTC TATG	SD
A_{10}	5'—CGATC TATTG/TEG/AGTGG CCCAT	SD
B_{11}	5'—TG TGTT GTGTC/TEG/TATGT TAAC GC	SD
B_{10}	5'—G TGTT GTGTC/TEG/TATGT TAAC G	SD
B_{9}	5'—TGTT GTGTC/TEG/TATGT TAAC	SD
B_{8}	5'—GTT GTGTC/TEG/TATGT TAA	SD
R_{12h}	5'—CTATTG AGTGGC TCATAC CGCGAT	SD
R_{11h}	5'—TATTG AGTGG TCCATA GCGATC	SD
R_{10h}	5'—TATTG AGTGG TCCAT CGATC	SD
$R_{10\_o\text{-}TEG}$	5'—TATTG AGTGG CCCAT/TEG/CGATC	SD
$P_{9\_i\text{-}TEG}$	5'—TAAC TGTT GTGTC/TEG/TATGT	SD
$P_{9\_o\text{-}TEG}$	5'—TAAC/TEG/TGTT GTGTC TATGT	SD
miDNA99a	5'—AA CCCGT AGATC CGATC TTGT G	SD

miDNA100	5’—AA CCCGT AGATC CGACC TTGT G	SD
miRNA99a	5’—AA CCCGU AGAUC CGAUC UUGU G	SD
miRNA100	5’—AA CCCGU AGAUC CGACC UUGU G	SD
R_{12_mi}	5’— CTTATTG GATCTA CGGGTT CGCGATC	SD
R_{11_mi}	5’—CTTATTG GATCTA CGGGT GCGATC	SD
R_{10_mi}	5’—TTATTG GATCT ACGGG CGATC	SD
$P_{9\_mi\_99a}$	5’—TAAC ACAA GATCG TATGT	SD
$P_{9\_mi\_100}$	5’—TAAC ACAA GTTCG TATGT	SD
Xf_inh	5’—GAT CTA TTG/TEG/CAG TGG CCC ATA CCC ATG C	SD
Xm_6_inh	5’ —TT G TGT/TEG/TAT GTT AAC	SD

[a]*teg*, triethylene glycol linkers; SD, standard desalting; BHQ1, black hole quencher 1; FAM, fluorescein label; SNS sites are underlined; self-complementary regions of MB probes are in italic, SNV and SNV-complementary nucleotides are in red.

3. Sencondary structure of the **inhC** analyte

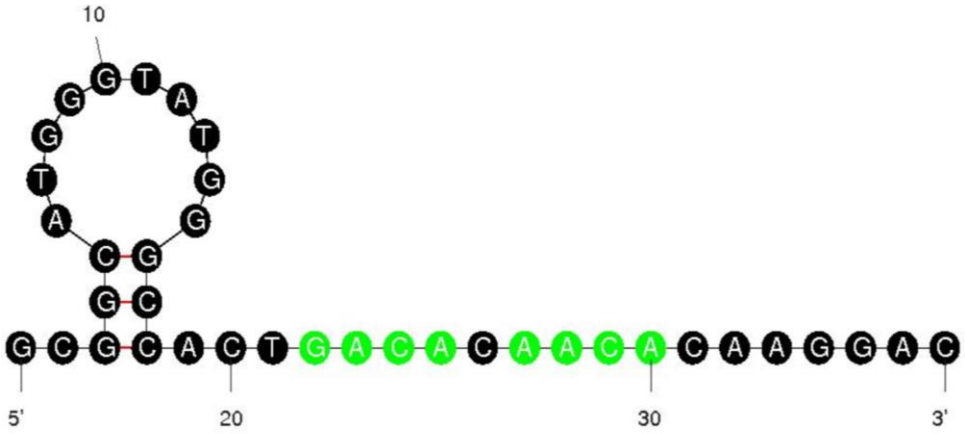

Figure S1. **Sencondary structure of the inhC analyte.** Lowest energy folding of the **inhC** analyte in mfold[5] shows a nearly linear structure. The green nucleotides indicate the region where $\mathbf{P_9}$ binds. The black nucleotide in the middle of the green region indicates the variable base (mismatch site); the **InhT** version of the analyte has a thymine in this position. The **InhC** and **InhT** analytes both have a $\Delta G = -1.84$ kcal/mol at 37°C when folded under the automatic mfold parameters.

4. Melting curves for $\mathbf{R_{10}/P_Y}$ Owl Sensors in comlex with **InhC** and **InhT** analytes

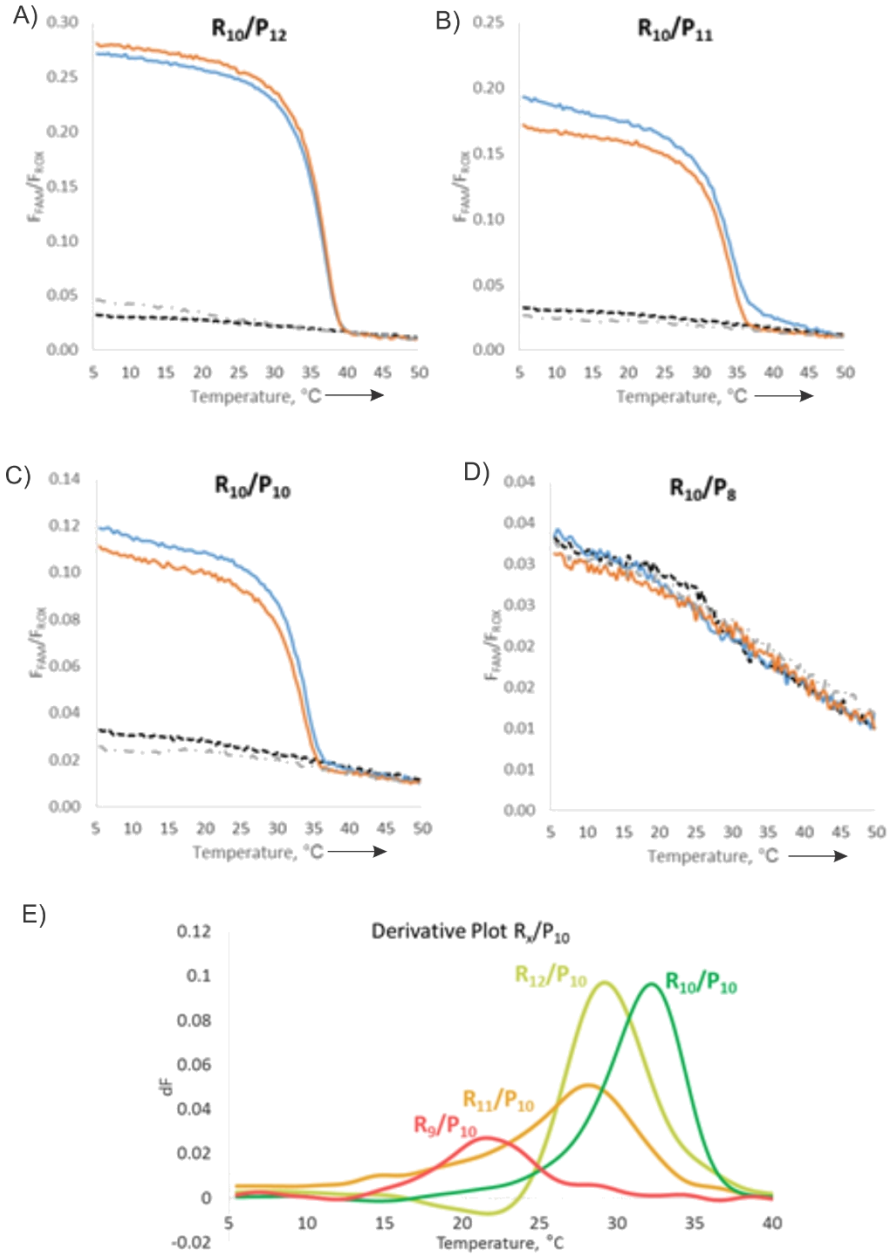

Figure S2. **Performance of Owl Sensor with different combinations of P and R strands.** Melting curves with R_{10}/P_X Owl Sensors and the derivative of the fluorescence of the matched analyte (panel E) shows the T_m at the peak of the curve. $\mathbf{R_{10}/P_{12}}$, $\mathbf{R_{10}/P_{11}}$ and $\mathbf{R_{10}/P_{10}}$ sensors are so stable that they do not differentiate well between matched **InhC** and mismatched **InhT** analytes (panels A, B and C). $\mathbf{R_{10}/P_8}$ sensor (panel D) is unstable since it does not produce fluorescence above the background in the prescence af matched analyte. The melt curve for $\mathbf{R_{10}/P_{10}}$ Owl Sensor shows high signal for both the matched (blue) and mismatched (orange) analytes, showing poor differentiation of a mismatch. This shows that $\mathbf{R_{10}/P_{10}}$ is the most stable structure of the $R_X/\mathbf{P_{10}}$ combinations tested. Unlike conventional probes, with our sensor design, additional nucleotides do not add to increased complex stability.

5. Melt curves complexes of **Rx/P9** (X =8,9,11,12) with **InhC** and **InhT** analytes

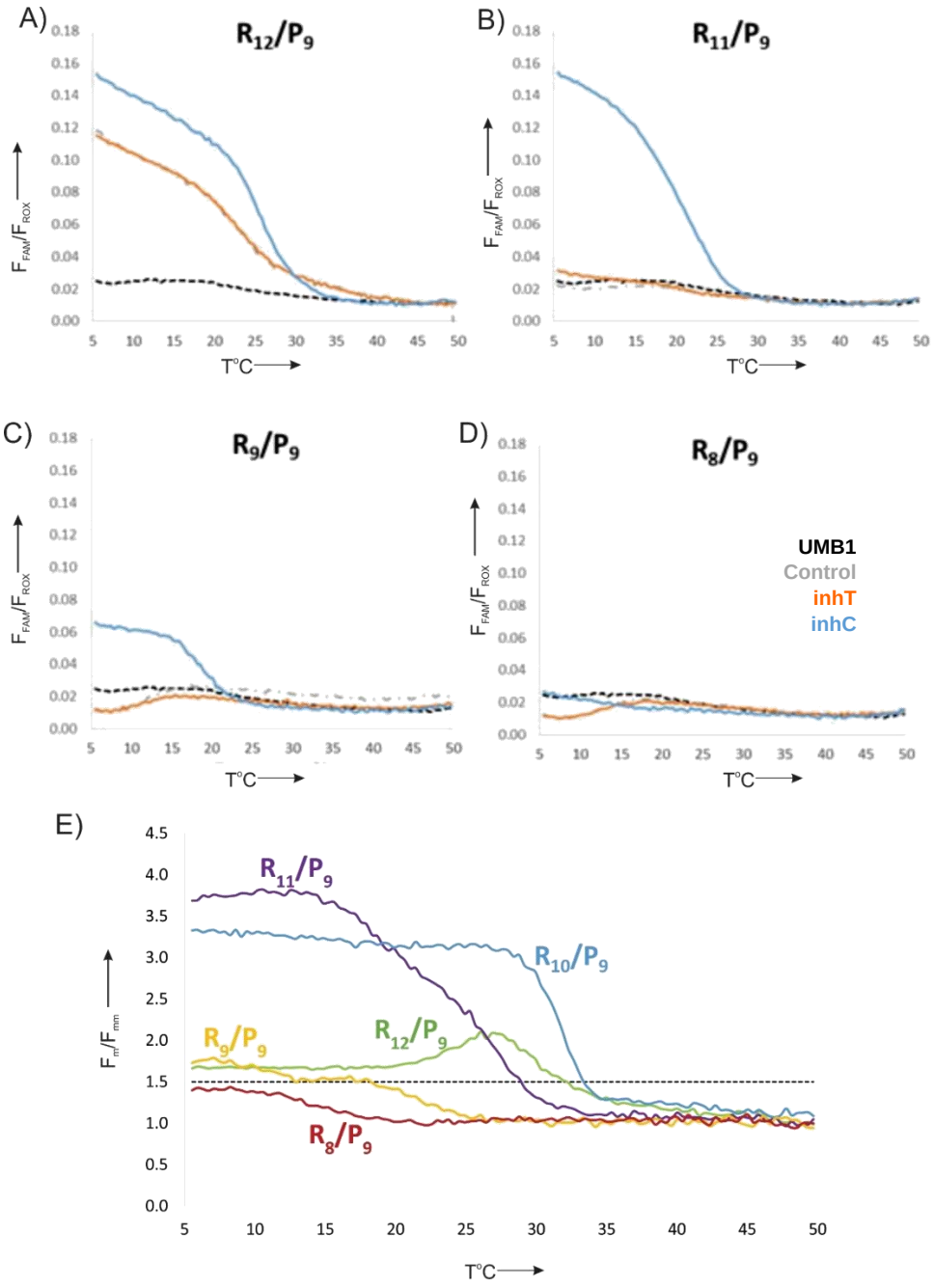

Figure S3. **R_{10}/P_9 produces the highest signal to background ratio and greatest diffrentataion of the mismatched InhT analyte**. E) By dividing the fluorescence of the matched analyte by the fluorescence of the mismatched analyte (F_M/F_{mm}) from Panels A-D, the differentiating power can be quantified. The green, purple, blue, yellow, and maroon lines represent **P_9** in combination with **R_{12}**, **R_{11}**, **R_{10}**, **R_9**, and **R_8**, respectively. Here we see that **R_{10}/P_9** shows the largest temperature range for differentiation, spanning 5-32°C. The horizontal line labeled $\Delta T_{1.5}$ indicates the cutoff line being used to determine differentiability.

6. Melting curves for MB and leaner probe - **Inh** analyte complexes

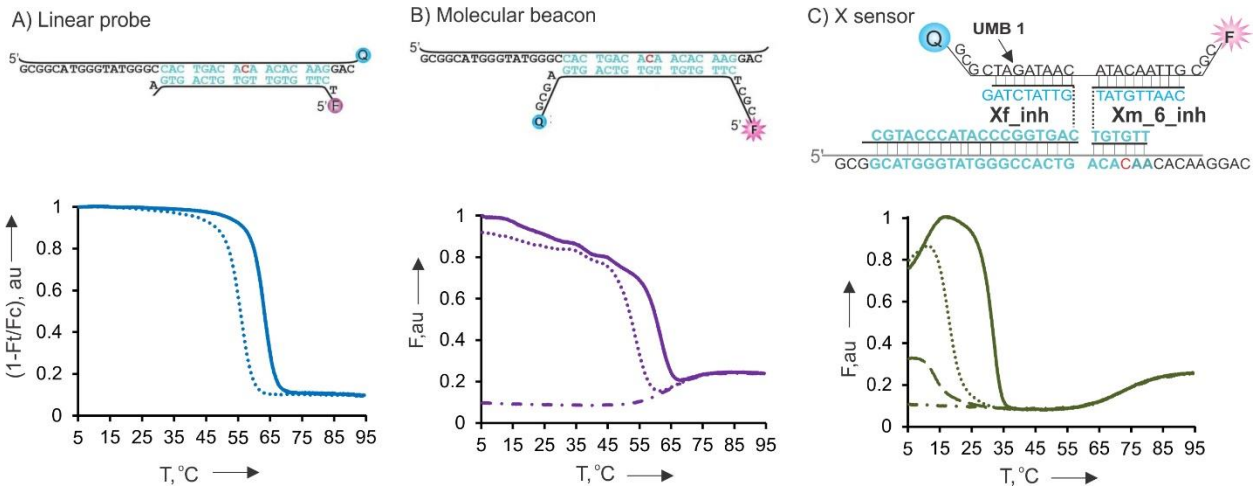

***Figure S4*. Fluorescence of the MB the Linear probe and X sensor in temperature interval 5-95ºC.** A) Linear probe. Upper panel: Linear probe hybridized to the matched analyte. The analyte was labeled by a quencher dye (Q), while the probe was conjugated with a fluorophore (F) to enable fluorescent detection of complex formation. Bottom panel: Reverse fluorescence (1-F) of the probe in the presence of matched Inh_C_Q (solid lines) and mismatched (dotted lines) Inh_T_Q analytes at different temperatures. The reverse fluorescence is presented to simplify comparison the data with panels B and C since linear probe, as designed, increased fluorescence upon melting, not decreasing as MB probe and X sensor. B)Molecular beacon probe. Upper panel: MB probe hybridizes to complementary target and produces fluorescent signal. The SNP position is shown in red, and the mutation is C ->T. Bottom panel: Melting temperature curves for specific MB probe. C) X sensor. Upper panel: Fluorescent crossover (X) complex formed by strands **Xf_inh** and **Xm_6_inh** when binding to analyte Inh_C and MB probe. MB-binding arms of strands f and m are in cyan. Bottom panel: Melting temperature curves for X sensors with 6-nucleotides long m-analyte binding (X_m-6_inh in Table 2).

7. Differentiation of SNV by the **R_{10}/P_9** Owl Sensor

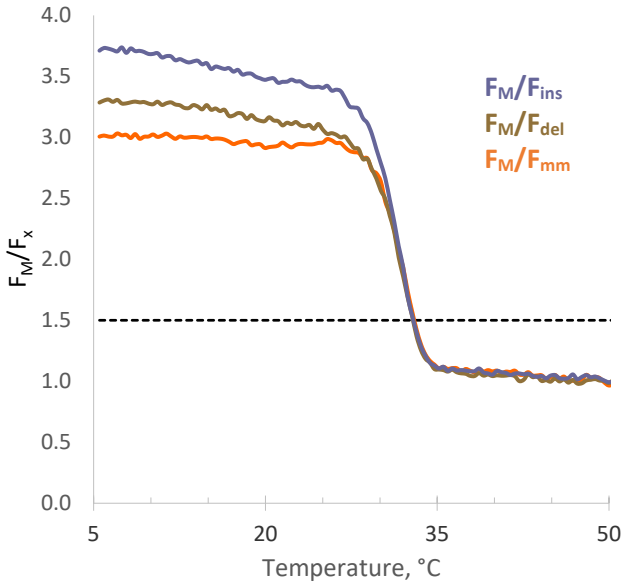

***Figure S5*. The R_{10}/P_9 Owl Sensor shows excellent selectivity with InhC and InhT analytes.** Differentiation ability for **R_{10}/P_9** with DNA analytes shows the Owl sensor can be assessed by graphing fluorescence of the matched analyte (F_M) divided by F_x, where F_x is the fluorescence of the insertion, deletion or mismatched analyte as indicated by F_i, F_d, and F_{mm}. Results show that excellent differentiation is achieved in the range 5-32.4°C. The black dashed line is $\Delta T_{1.5}$, the standard for differentiation, set at F_M/F_x being greater than or equal to 1.5.

8. Selectivity of **R_{10}/P_{9_A}** specific to **InhT** analyte

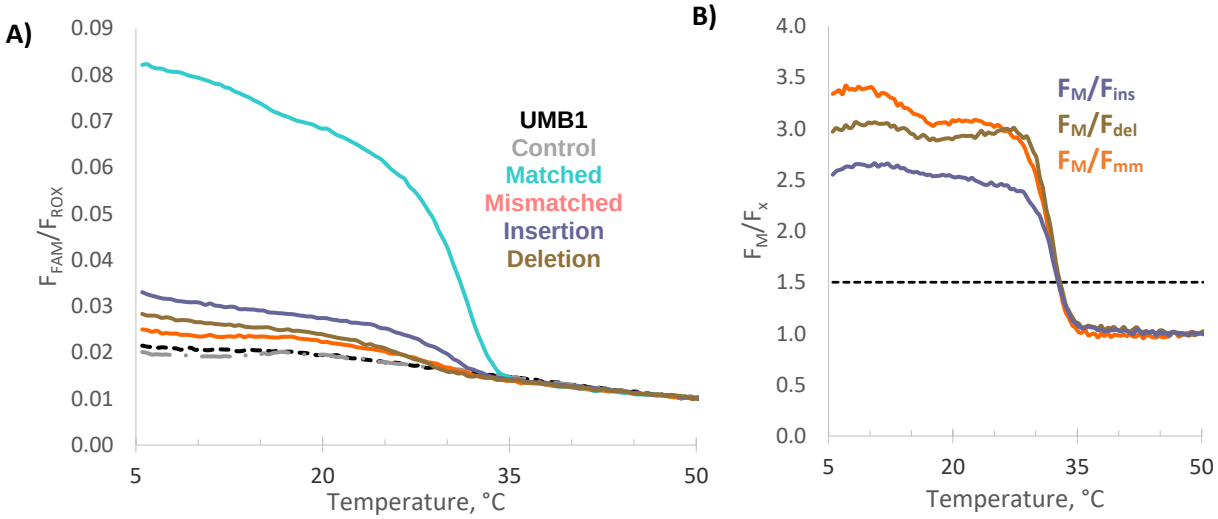

Figure S6. **Owl Sensor specific to InhT DNA shows excellent performance.** A) Melt Curve for R_{10}/P_{9_A} sensor the **InhT**-specific Owl Sensor, with DNA analytes shows high signal for the matched analyte (teal line) with minimal signal for insertion (purple line), deletion (brown line), and mismatched (orange) analytes. The signal from **UMB1** alone is represented by the black dashed line, and the signal from the control (**UMB1** with **R_{10}** and **P_{9_A}**) is represented by the grey dotted dashed line. B) Differentiation ability for R_{10}/P_{9_A} sensor with DNA analytes shows the Owl Sensor can be assessed by graphing F_M/F_x. Results show that differentiation is achieved up to 32.6°C for all SNVs tested.

9. Limit of Detection for the $\mathbf{R_{10}/P_9}$ Owl Sensor

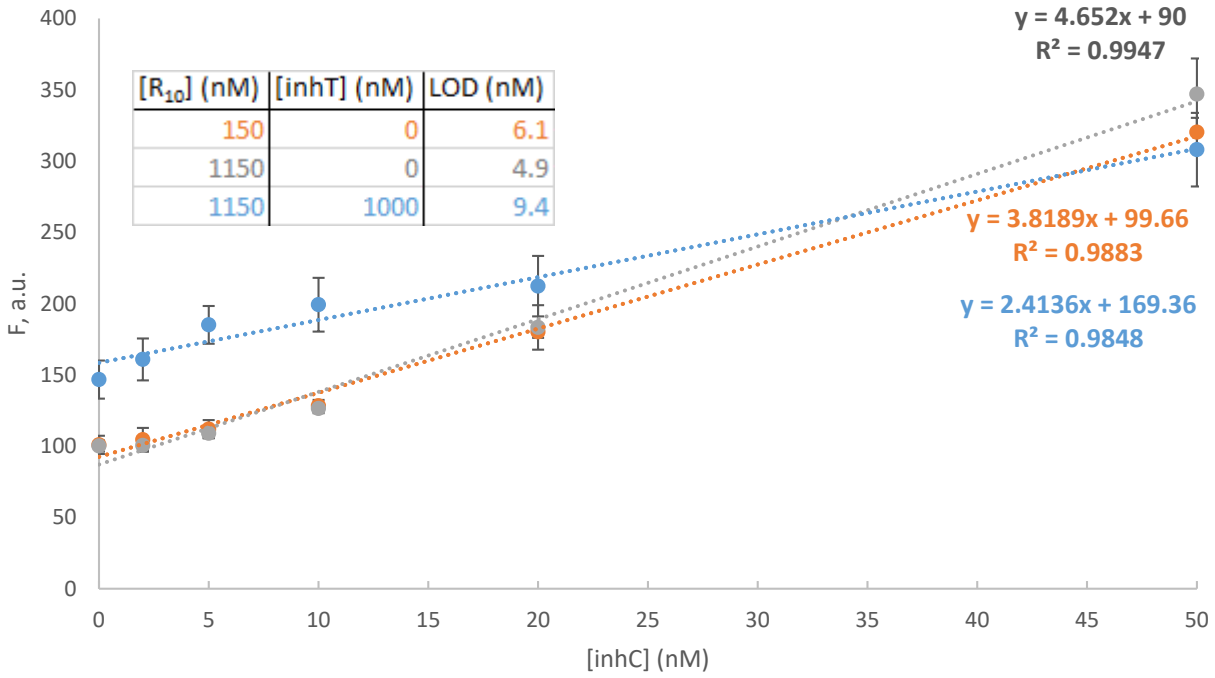

Figure S7. **Limit of detection (LOD) for the $\mathbf{R_{10}/P_9}$ Owl Sensor.** The inset shows the concentration of $\mathbf{R_{10}}$, **InhC** (matched), and **InhT** (mismatched) and the LOD for each of the three samples. The orange line represents the LOD for the same concentrations of oligonucleotides as the melt curves. The blue line shows the LOD for the Owl Sensor when a large excess of **InhT** (mismatched) analyte is present. This shows that the $\mathbf{P_9}$ strand did not hybridize large amounts of excess nonspecific analyte, and shows that the correct analyte can be detected even with mismatched analyte at over 100 times excess concentrations. Since $\mathbf{R_{10}}$ binds to an unchanged region of the *inhA* analyte (its analyte binding domain is fully complementary to **InhC** and **InhT**), high concentrations of $\mathbf{R_{10}}$ were used (1.15 µM) so that enough $\mathbf{R_{10}}$ was available to bind both **InhC** and the large excess of **InhT**. For comparison, LOD with 1.15 µM of $\mathbf{R_{10}}$ was also found to be 4.9 nM (grey line).

10. Differentiation of the Owl Sensor with outside TEG Linkers.

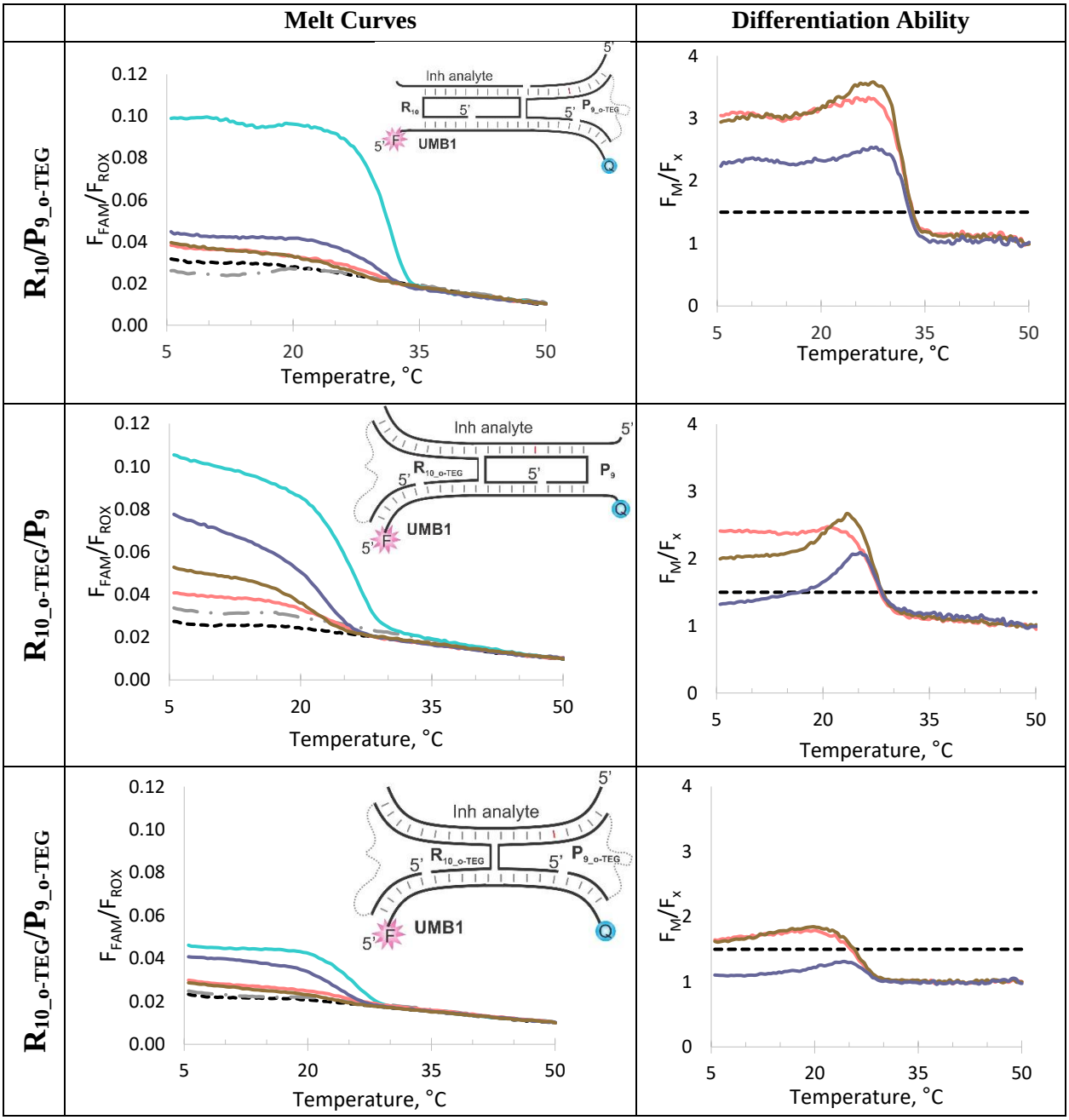

Figure S8. **Differentiation of the Owl Sensor with TEGs on the outside junctions.** Melting curves and differentiation are shown for the Owl Sensor with outside TEG linkers in the **P**, **R**, and both adapter strands (o-TEG). For melting curves, the fluorescence of the matched, insertion, deletion, and mismatched analyte is shown in cyan, purple, brown, and peach, respectively. For differentiation graphs, the fluorescence of the matched was divided by that of the insertion, mismatch, or deletion analyte and is shown in purple, orange, or brown, respectively. Drawings of the Owl Sensor with TEG linkers are shown as insets to the melt curves. The melt curves for the **R**$_{10\_o\text{-}TEG}$/**P**$_{9\_o\text{-}TEG}$ show overall very low fluorescence for the complex (SI

Table 1). This is likely due to low complex formation and because flexibility on the outside of the sensor allows for the possibility of the ends of the complex bending around. Results show that adding flexibility to the outside junction of $\mathbf{P_9}$ ($\mathbf{P_{9\_o\text{-}TEG}}$) did not significantly affect the differentiation ability or complex stability and even slightly increased the fluorescent value at 5°C for the matched analyte when compared to that of R_{10}/P_9 or R_{10}/P_{9_A} sensors (the $\mathbf{P_{9\_A}}$ was specific to the mutant **inhT** analyte). A possible reasoning for this is that the flexibility on the outside of the P_9 strand allows for a reduction in the strain of the complex caused by non-ideal exit trajectories into the flexible TEG linker.

Adding TEG linkers increased the entropy of the adapter strands, especially when unbound, and according to the equation $\Delta G=\Delta H-T\Delta S$, increasing the entropy results in a more negative ΔG. If the TEG linker is on the outside of the Owl Sensor complex, as is the case for strands with outside and double TEGs, not only is the entropy of the reactants increased due to having more flexible free DNA strands, but the entropy of the products increases, as the formed Owl Sensor complex is able to more easily bend out of plane (See drawings SI Tables 2 and 4). While the ends of the helices of the regular Owl Sensor are tethered with little flexibility or freedom for movement, the outside and double TEG linkers allow for the helices to adopt non-parallel helices due to the increased flexibility, which is associated with higher entropy of the complex.

Contrastingly, having only one inside TEG linker does not significantly increase the flexibility of the system. Therefore, adding flexibility into only one inside junction of the Owl Sensor will increase the stability of the dissociated state, as the entropy of the free strand will increase without adding much entropy into the formed complex, resulting in low complex formation and a reduction in the stability of the associated state, as expressed by a low T_m.

While it is unclear how to explain the mechanism of complex destabilization and loss of differentiation behind each combination of the $\mathbf{R_{10}/P_9}$ strands, it can be generally stated for the Owl Sensor that a rigid structure is optimum for a large temperature range for differentiation of SNVs.

11. Differnetiation of the Owl Sensor with inside TEG Linkers

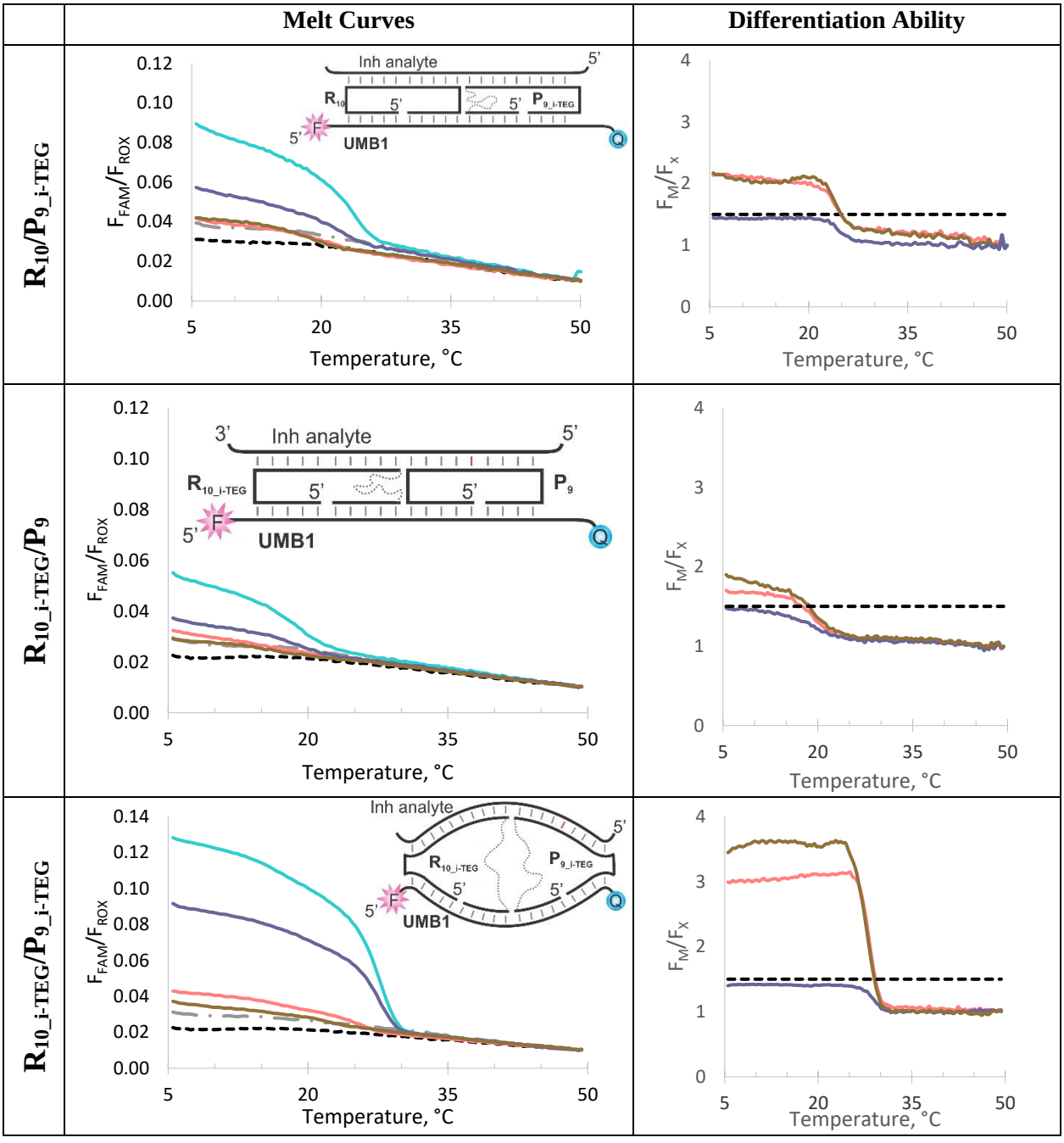

Figure S9. **Differentiation of the Owl Sensor with TEGs on the inside junctions.** Melt curves and differentiation is shown for the Owl Sensor with inside TEG linkers in the **P**, **R**, and both adapter strands (i-TEG). For melt curves, the fluorescence of the matched, insertion, deletion and mismatched analyte is shown in cyan, purple, brown, and peach, respectively. For differentiation graphs, the fluorescence of the matched was divided by that of the insertion, mismatch, or deletion analyte and is shown in purple, orange, or brown, respectively. Drawings of the Owl Sensor with TEGs are shown as insets to the melt curves.

12. Differentiation of the Owl Sensor with inide and ouside TEG Linkers

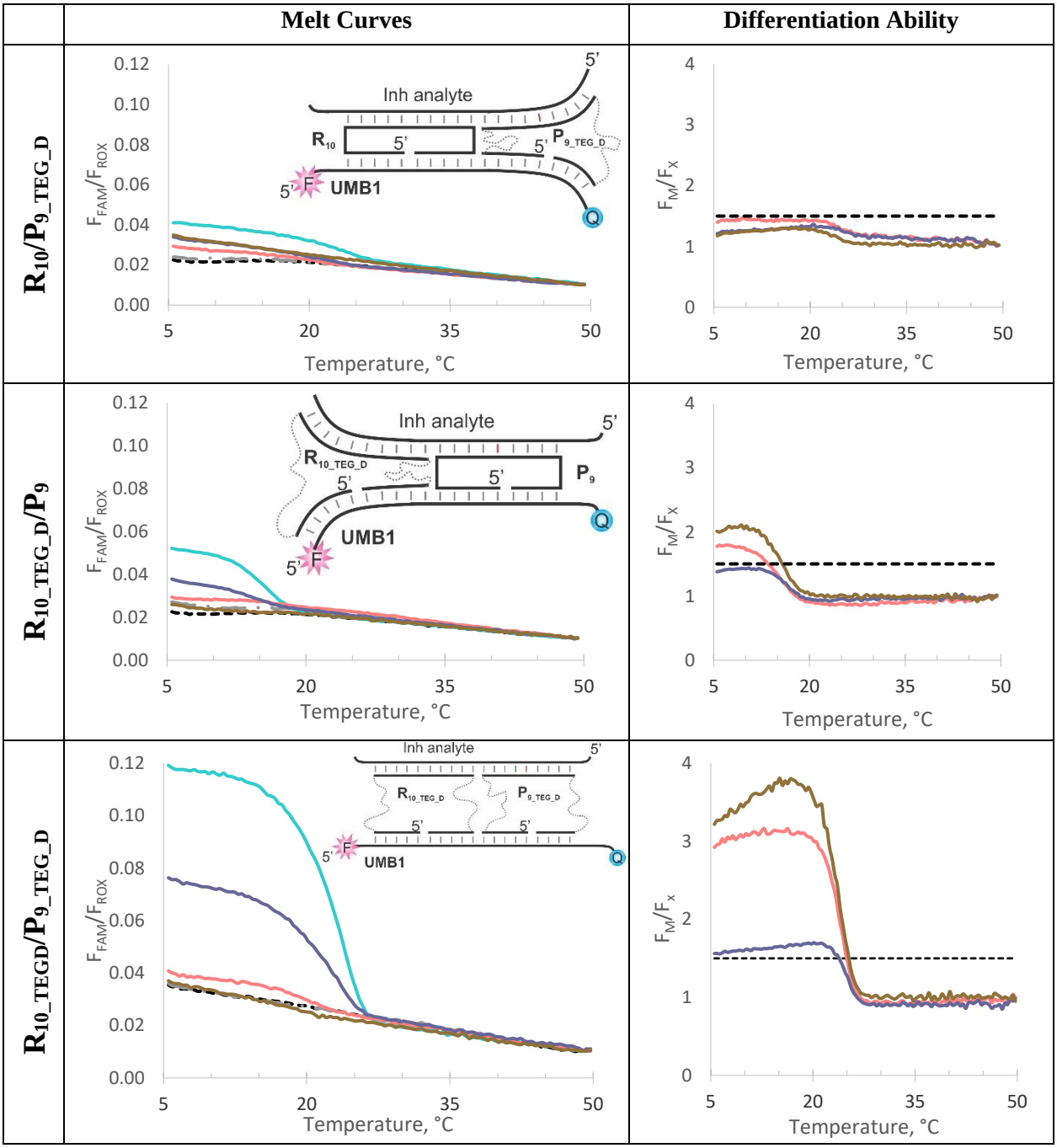

Figure S10. **Differentiation of the Owl Sensor with TEG linkers on the both junctions.** Melt curves and differentiation are shown for the Owl Sensor with TEG linkers on the inside and outside of **P**, **R**, and both adapter strands (TEGD). For melt curves, the fluorescence of the matched, insertion, deletion, and mismatched analyte is shown in cyan, purple, brown, and peach, respectively. For differentiation graphs, the fluorescence of the matched was divided by that of the insertion, mismatch, or deletion analyte and is shown in purple, orange, or brown, respectively. Drawings of the Owl Sensor with TEGs are shown as insets to the melt curves.

13. ***Table S2.*** Temperature differentiation ranges for Owl Sensor and other probes

Probe	T_{low}	T_{high}	$\Delta T_{1.5}$
Linear Probe	46.8	62.4	15.6
Molecular Beacon	51.1	65.9	14.8
X sensor	16.2	35.0	18.8
Owl Sensor	5.0	32.4	27.4

The differentiation by each of the sensors. T_{low} is the lowest temperature where differentiation can be achieved. T_{high} is the highest temperature in which differentiation is achieved. The $\Delta T_{1.5}$ is calculated by T_{high}-T_{low}.

14. ***Table S3***. Differentiation Ranges for Owl Sensor R_X/P_9.

x	$\Delta T_{1.5}$	Temperature Range (°C)
12	26.9	5.0-31.9
11	23.8	5.0-28.8
10	27.0	5.0-32.4
9	12.9	5.0-17.9
8	0.0	--

.

The largest temperature range for analyte differentiation is with the R_{10}/P_9 Owl Sensor with DNA analytes.

15. Diffrentiation of **Inh_C** and **Inh_T** anlytes by X sensor

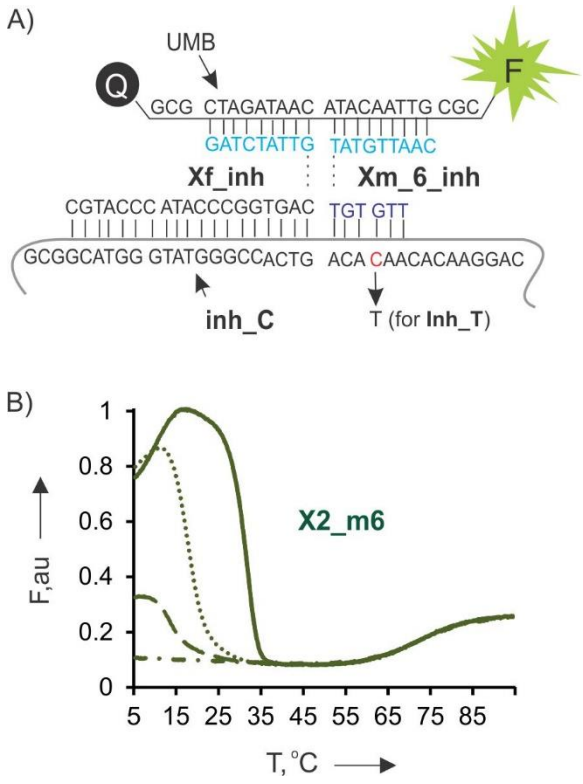

Figure S11. **Recognition of InhC and Inh T analytes by compelmentary X sensor.** A) Hybridization of X sensor to **InhC**. A 'c' at SNS position is red. B) Melting curves of corresponding complexes InhC (solid line) and Inh_T (dotted line) compelxes with X sensor. Dashed line – X sensor without aanlyte; dashed-dotted line: **UMB1** anly controls. The reaction mixtures contain 50 mM Tris-HCl (pH = 7.4), 100 mM $MgCl_2$, 0.1% Tween 20, 50 nM **UMB1**, 200 nM **Xf_inh**, and 120 nM **Xm_6_inh**.

16. Owl sensors performance with RNA Inh-related analytes

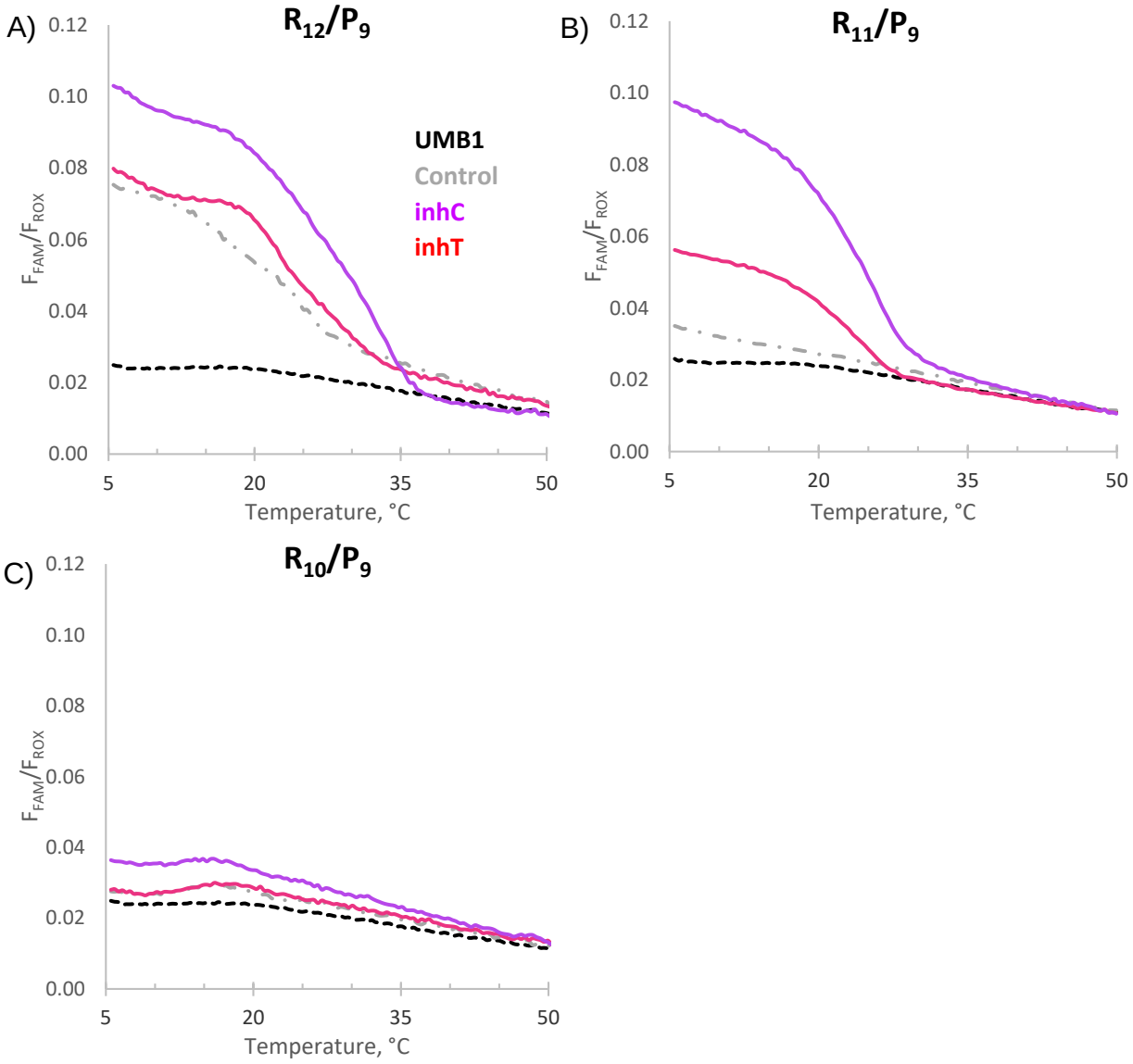

Figure S12. **R_{11}/P_9 is the best Owl Sensor for differentiating SNPs in RNA analytes.** Assays done at 50 mM $MgCl_2$. A) Melt Curve for R_{12}/P_9 with RNA analytes shows little differentiation. B) Melt Curve for R_{11}/P_9 with RNA analytes shows the best differentiation for matched and mismatched analytes. C) Melt Curve for R_{10}/P_9 with RNA analytes shows minimal complex formation.

17. Owl Sensor optimized performance with RNA Inh-related analytes.

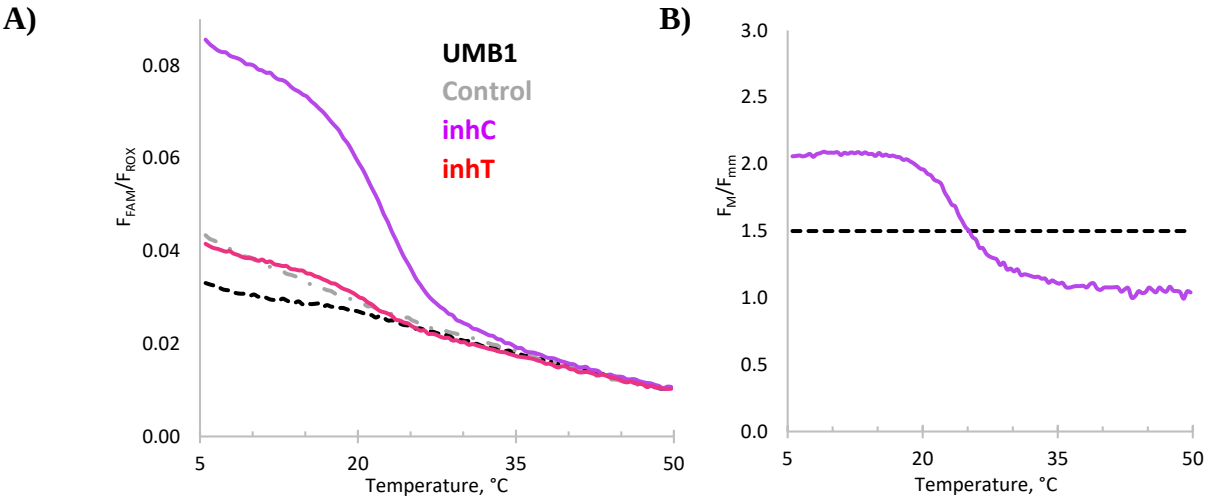

***Figure S13*. The Owl Sensor is able to differentiate mismatches in RNA analytes.** A) Melt Curve for R_{11}/P_9 sensor with *inhA* RNA analytes. B) Differentiation ability for R_{11}/P_9 sensor with RNA analytes extends from 5-25.1°C using 10 mM $MgCl_2$.

In order to increase differentiation between matched and mismatched analytes, $MgCl_2$ concentrations were optimized to 10 mM.

18. Structures of Owl Sensors in complex with **miDNA99a** analytes

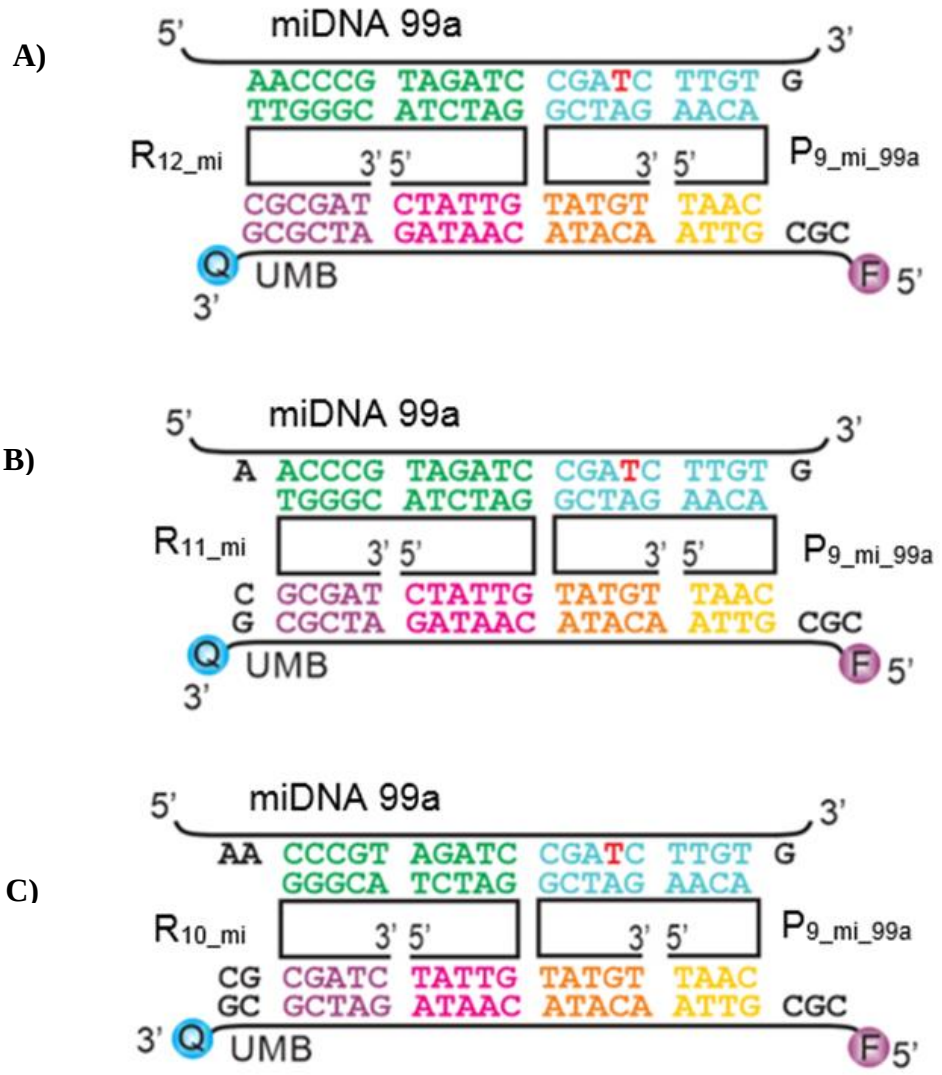

Figure S14. **Structures of Owl Sensors in complex with miDNA99a analytes.**

19. Secondary Structures of **miDNA99aa** and **miDNA100**

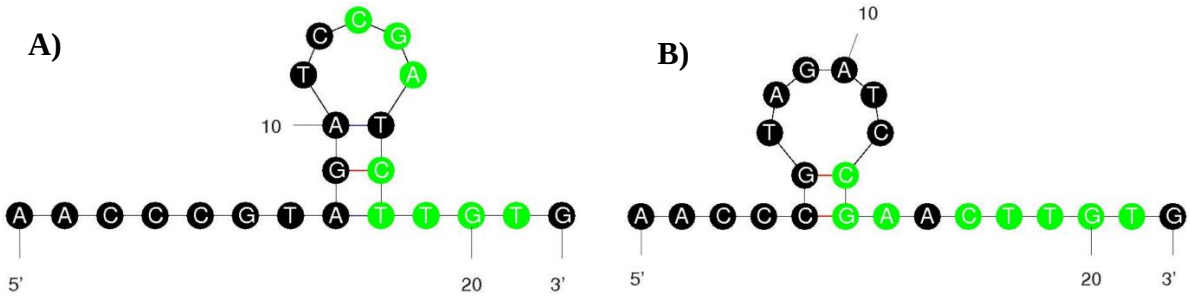

Figure S15. **Secondary structures of miDNA analytes.** The (A) **miDNA99a** (ΔG= – 0.91 kcal/mol) and (A) **miDNA100** (ΔG= – 0.14 kcal/mol) analytes are shown folded at 37°C when folded under the automatic mfold parameters.[22] The green nucleotides indicate the region where $\mathbf{P_{9\_mi}}$ binds. The black nucleotide in the middle of the green region indicates the variable base.

20. Melting temperature of diffrente Owl semsors with **miDNA** analytes.

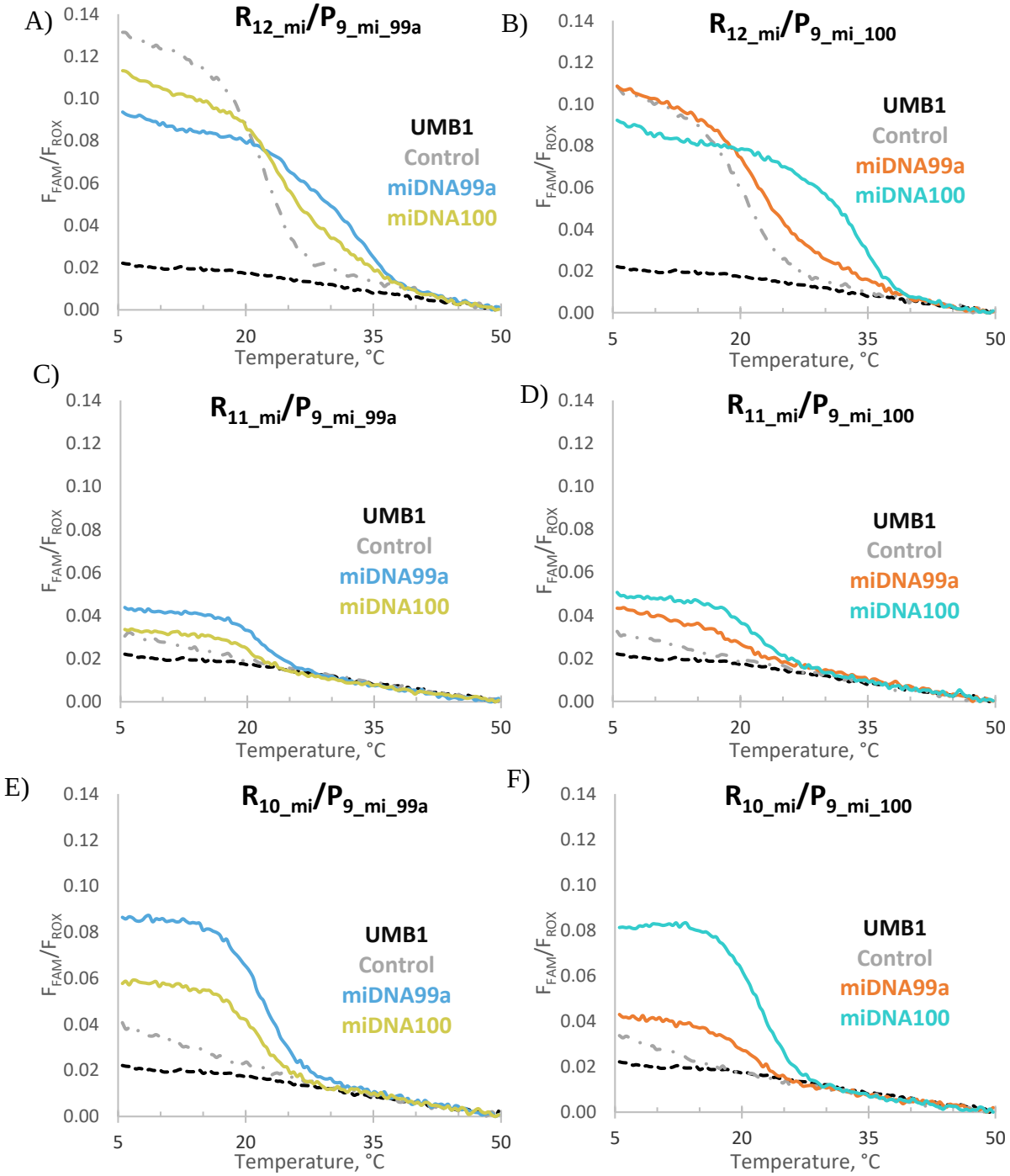

Figure S16. **Melt curves for Owl Sensor specific to miDNA.** Figures A, C, and D show melt curves for an R strand with 12-10 nt analyte binding arms with a P_9 specific to **miDNA99a**. Panels B, D, and F show differentiation for an R strand with 12-10 nucleotides for R paired with a P_9 specific to **miDNA100.** Owl Sensors with $\mathbf{R_{12\_mi}}$ and $\mathbf{R_{11\_mi}}$ show poor differentiation between matched and mismatched DNA analytes. Here we see again that an R strand that is 10 nucleotides long is best for differentiating mismatches when analyzing DNA analytes. The buffer used contained 50 mM Tris-HCl pH 7.4, 50 mM $MgCl_2$, and 0.1% Tween-20.

21. Optimized melting temperature conditions for **miDNA** analytes

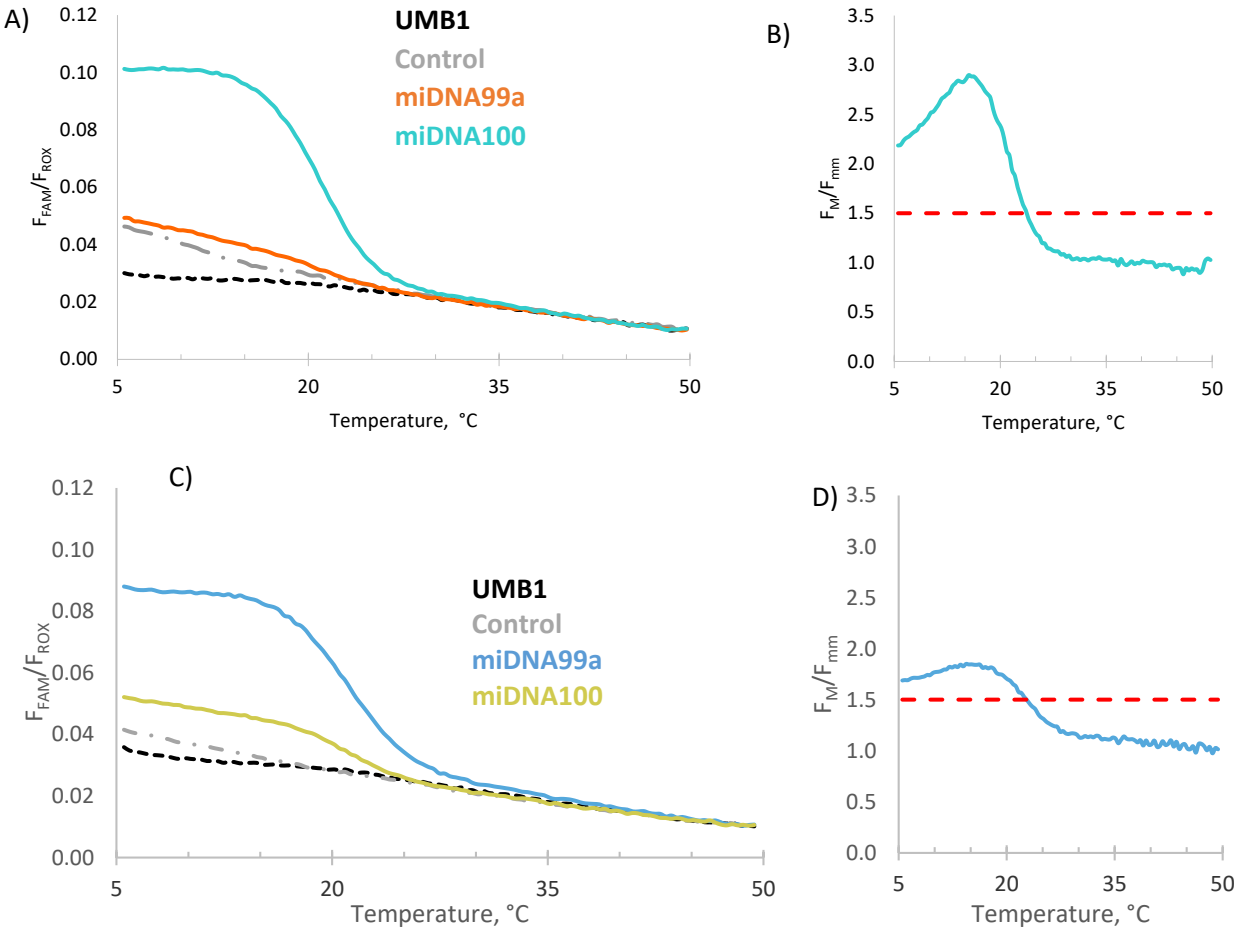

Figure S17. **Optimized melt curves and differentiation of DNA analytes with the $R_{10\_mi}/P_{9\_mi\_100}$ and $R_{10\_mi}/P_{9\_mi\_99a}$ Owl Sensors.** A) The melt curve for $R_{10\_mi}/P_{9\_mi\_100}$ Owl Sensor (specific to **miDNA100** and mismatched with **miDNA99a**) shows excellent differentiation between the matched (teal) and mismatched (orange) analytes. B) The differentiation range extends from 5-23.2°C for Owl Sensor $R_{10\_mi}/P_{9\_mi\_100}$ Owl Sensor with DNA analytes. C) The melt curve for **$R_{10\_mi}/P_{9\_mi\_99a}$** Owl Sensor (specific to **miDNA99a** and mismatched with **miDNA100**) shows excellent differentiation between the matched (blue) and mismatched (mustard) analytes. D) The differentiation range extends from 5-22.4°C for Owl Sensor $R_{10\_mi}/P_{9\_mi\_99a}$ Owl Sensor with DNA analytes. The buffer used contained 50 mM Tris-HCl pH 7.4, 40 mM $MgCl_2$, and 0.1% Tween-20.

22. Owl Sensors performance with **miRNA99** and **miRNA100** analytes.

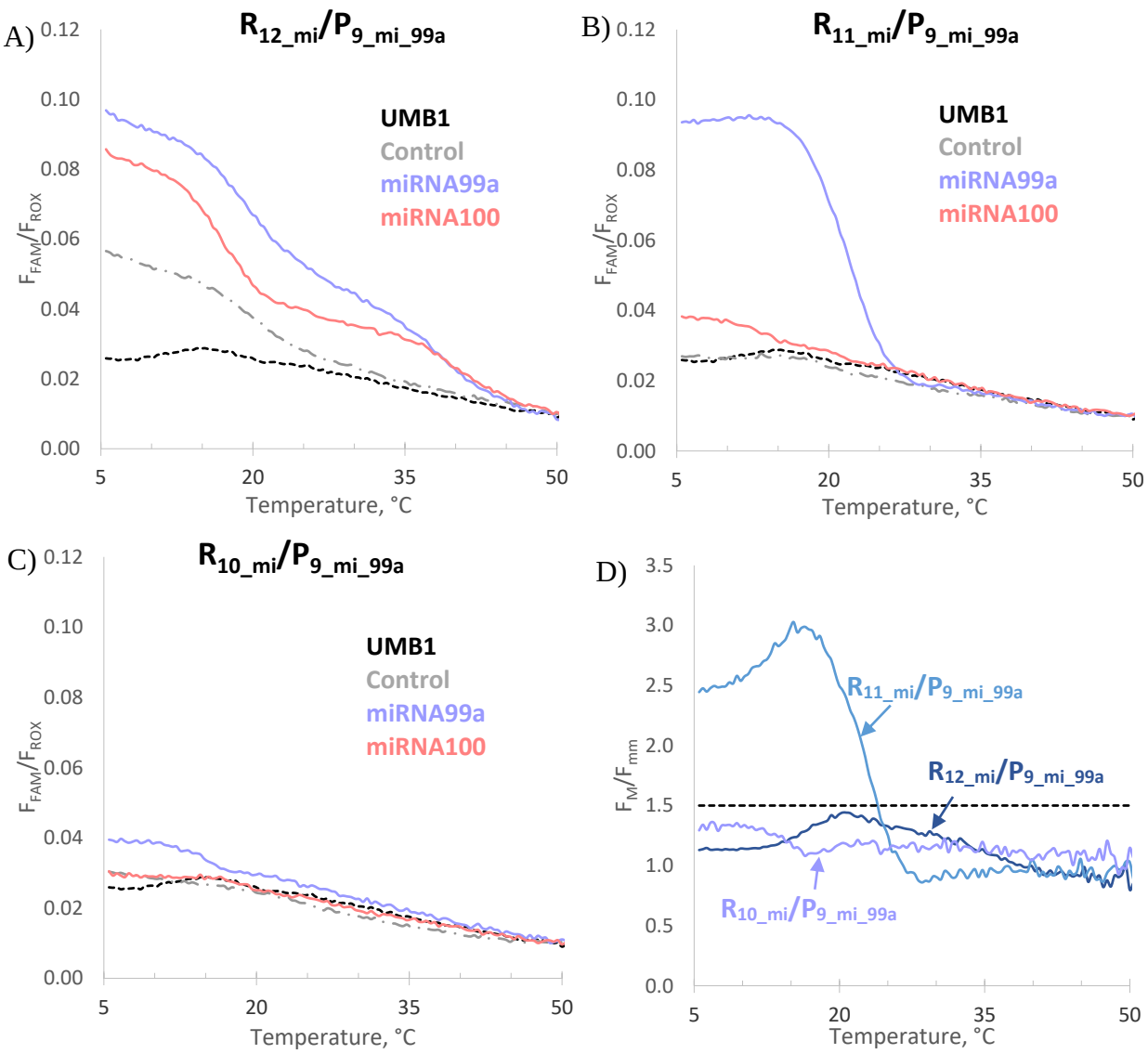

Figure S18. **R_{11_mi} is the best R length for differentiating the mismatched analyte in miRNA analytes**. A, B and C) The melt curves for UMB, the Control, **miRNA99a**, and **miRNA100** are represented by the black dashed, grey dotted dashed, coral, and purple lines, respectively. D) The differentiation range for Owl Sensor $R_{11\_mi}/P_{9\_mi\_99a}$ Owl Sensor with RNA analytes. The buffer used contained 50 mM Tris-HCl pH 7.4, 40 mM $MgCl_2$, and 0.1% Tween-20.

23. Optimized melt curves and differentiation of miRNA Analytes

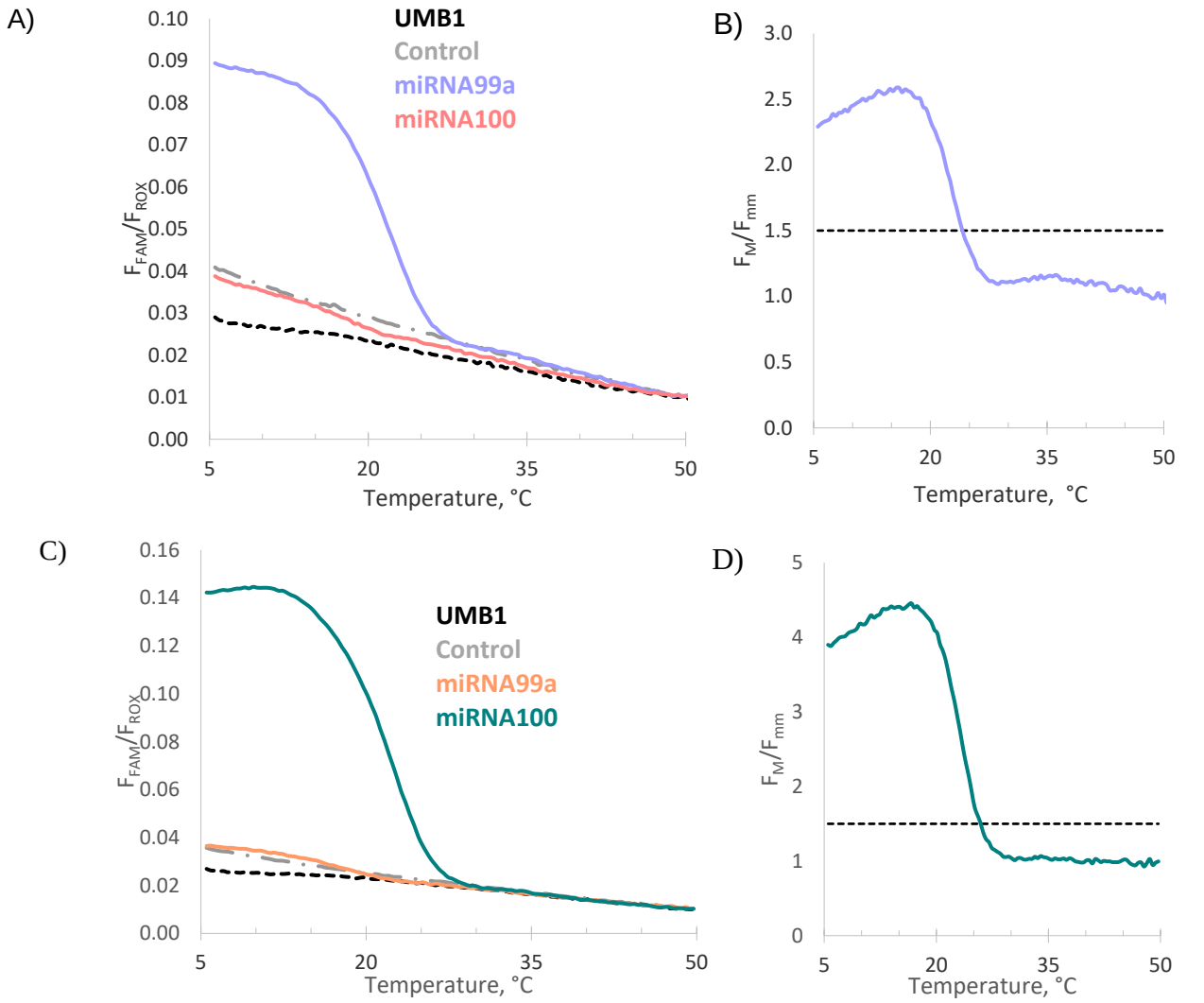

Figure S19. **Optimized melt curve and differentiation of miRNA Analytes**. A) The melt curve for $\mathbf{R_{11\_mi}/P_{9\_mi\_99a}}$ shows excellent differentiation between the matched (purple) and mismatched (salmon) analytes. B) The differentiation range for Owl Sensor $\mathbf{R_{11\_mi}/P_{9\_mi\_99a}}$. Owl Sensor with RNA analytes differentiates in the temperature range 5-25.7°C. C) The melt curve for $\mathbf{R_{11\_mi}/P_{9\_mi\_100}}$ shows excellent differentiation between the matched (teal) and mismatched (orange) analytes. D) The differentiation range for Owl Sensor $\mathbf{R_{11\_mi}/P_{9\_mi\_100}}$ Owl Sensor with RNA analytes extends from 5-24.1°C. The buffer used contained 40 mM Tris-HCl pH 7.4, 40 mM $MgCl_2$, and 0.1% Tween-20**.**

24. Effect of the prescenc of random RNA on the performance of Owl Sensor.

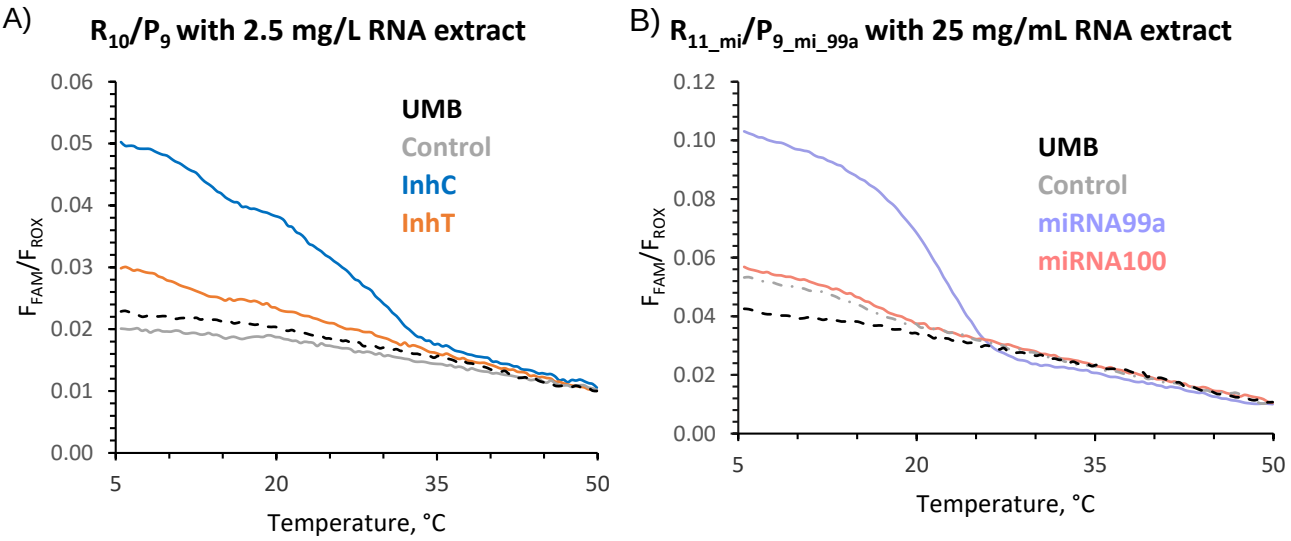

***Figure S20*. Performance of Owl sensors in the presence of radmom RNA.** A) Melting curves for **R_{10}/P_9** Owl Sensor (R10: 5'-TAT TGA GTG GCC CAT CGA TC, P9: 5'- TAA CTG TTG TGT CTA TGT; and UMB1, 5'-/FAM/-CGC GTT AAC ATA CAA TAG ATC GCG-/BHQ1/) in the presence of fully matched **InhC** or mismatched InhT (orange). Grey dotted-dashed line: no analyte control; black dashed line: **UMB1** only. The samples contained 50 mM Tris-HCl, pH 7.4, 50 mM $MgCl_2$, and 0.1% Tween-20 with 50 nM UMB1, 50 nM ROX, 150 nM R10, 200 nM P9, 2.5 mg/L *S.cerevisiae* RNA (Sigma, R8759) and 100 nM analytes. B) Melting curves of the complex of **R_{11}/P_9** with fully matched **miRNA99a** or missmatched **miRNA100**. Owl Sensor The samples contained 50 mM Tris-HCl, pH 7.4, 50 mM $MgCl_2$, and 0.1% Tween-20 with 50 nM **UMB1**, 50 nM ROX, 150 nM R10, 200 nM P9, 25 mg/L S.cerevisiae RNA (Sigma, R8759) and 100 nM analytes. ROX dye was used as an internal control for normalization of fluorescence from different samples.

25. References

1. Tyagi, S.; Kramer, F. R. Nat. Biotechnol. 1996, 14, 303−308.
2. Kolpashchikov, D. M. Scientifica 2012, 2012, 928783.
3. Tsourkas, A.; Behlke, M. A.; Bao, G. Nucleic Acids Res. 2002, 30, 4208−4215.
4. http://www.molecular-beacons.org/MB_SC_design.html
5. http://unafold.rna.albany.edu/?q=mfold/dna-folding-form